

## A UNIFIED SOLUTION FOR THE ORBIT AND LIGHT-TIME EFFECT IN THE V505 Sgr SYSTEM

M. BROŽ<sup>1</sup>, P. MAYER<sup>1</sup>, T. PRIBULLA<sup>2,4</sup>, P. ZASCHE<sup>1</sup>, D. VOKROUHICKÝ<sup>1</sup>, AND R. UHLÁŘ<sup>3</sup>

<sup>1</sup> Astronomical Institute, Charles University, Prague, V Holešovičkách 2, 18000 Prague 8, Czech Republic

<sup>2</sup> Astrophysikalisches Institut und Universitäts-Sternwarte, Schillergässchen 2-3, D-07740 Jena, Germany

<sup>3</sup> Private Observatory, Pohoří 71, 25401 Jílové u Prahy, Czech Republic

Received 2010 February 4; accepted 2010 March 28; published 2010 April 19

### ABSTRACT

The multiple system V505 Sagittarii is composed of at least three stars: a compact eclipsing pair and a distant component, whose orbit is measured directly using speckle interferometry. In order to explain the observed orbit of the third body in V505 Sagittarii and also other observable quantities, namely the minima timings of the eclipsing binary and three different radial velocities (RVs) detected in the spectrum, we thoroughly test a fourth-body hypothesis—a perturbation by a dim, yet-unobserved object. We use an  $N$ -body numerical integrator to simulate future and past orbital evolution of three or four components in this system. We construct a suitable  $\chi^2$  metric from all available speckle-interferometry, minima-timings, and RV data and we scan a part of a parameter space to get at least some of the possible solutions. In principle, we are able to explain all observable quantities by the presence of a fourth body, but the resulting likelihood of this hypothesis is very low. We also discuss other theoretical explanations of the minima-timing variations. Further observations of the minima timings during the next decade or high-resolution spectroscopic data can significantly constrain the model.

**Key words:** binaries: close – stars: individual (V505 Sgr)

**Online-only material:** color figures

### 1. INTRODUCTION

The star V505 Sagittarii (HD 187949, HR 7571, HIP 97849, WDS 19531-1436) is known as an eclipsing binary with a variable period. Spectral types of its primary and secondary components are A2 V and G5 IV, orbital period is 1.183 days, and visual magnitude is maximum 6<sup>m</sup>5 (Chambliss et al. 1993). In 1985, the V505 Sgr was also resolved using speckle interferometry (McAlister et al. 1987b), and several measurements of the third component were published since that time. Mayer (1997) attempted to join the measured times of minima with visual orbit and determined a distance of the system 102 pc.

The third-body orbit with the period of about 40 years seemed well justified until about the year 2000. An abrupt change in more recent data, however, excludes this simple model—it is impossible to fit both light-time effect data and the interferometric trajectory assuming three bodies on stable orbits. We thus test a fourth-body hypothesis: a perturbation by a low-mass star (i.e., the fourth body), which has not been resolved spatially so far. Such a fourth body was suspected already by Chochol et al. (2006) due to conspicuous deviations of minimum times from those expected. While we consider the fourth-body model as the main working hypothesis in this paper, we also discuss other possible effects that can produce minima timing variations.

The data set we have for V505 Sgr is described in Section 2. We introduce our dynamical model, numerical method, free/dependent parameters, and  $\chi^2$  metric in Section 3. The results of our simulations and conclusions are presented in Sections 4 and 5.

### 2. OBSERVATIONAL DATA

#### 2.1. Speckle Interferometry

The available speckle-interferometry data are summarized in Table 1. Most of them were extracted from the Fourth Catalog of Interferometric Measurements of Binary Stars (Hartkopf et al. 2009), but we also added two speckle measurements from the SAO BTA 6 m telescope by E. Malogolovets (using a speckle camera and a method described in Balega et al. 2002 and Maksimov et al. 2009) and one direct-imaging measurement, performed at CFHT by S. Rucinski (using a method described in Rucinski et al. 2007).

We estimated weight factors  $w$  and corresponding uncertainties as  $\sigma_{\text{sky}} = 0.005 \text{ arcsec}/w$ . This uncertainty refers to the measured position on the plane of the sky ( $X^2 + Y^2$ ), which results from a combination of uncertainties in the measured angular separations and position angles. The values of  $\sigma_{\text{sky}}$  vary because different telescopes and techniques were used. Any non-monotonic changes in the measured position angles are simply due to observational uncertainties.

We are aware of a possible 180° ambiguity in the speckle measurements, but V505 Sgr is a lucky case: we have one direct measurement by *Hipparcos* prior to 2000 perihelion passage, and another direct-imaging datum after 2000. We thus can be sure about the shape of the orbit.

#### 2.2. Minima Timings

We list recent  $O - C$  data for the (1+2) binary in Table 2. Only measurements not presented in Chambliss et al. (1993) are included in the table, but we use all of them of course. An uncertainty of a minimum determination is estimated to be  $\sigma_{\text{lite}} = 1 \text{ minute}$  in most cases, only photographic minima and data from *Hipparcos* were considered worse. Epoch and  $O - C$  were calculated using the ephemeris of Mayer (1997), with zero

<sup>4</sup> On leave from Astronomical Institute, Slovak Academy of Sciences, 05960 Tatranská Lomnica, Slovakia.

**Table 1**  
Speckle-interferometry Data for V505 Sgr, Mainly from the Fourth  
Interferometric Catalogue (Hartkopf et al. 2009)<sup>a</sup>

Year	P.A. (deg)	$\rho$ (mas)	Weight	Source
1985.5150	189.6	302	1	3.6 m
1985.8425	189.8	311	1	3.8 m
1989.3069	181.0	261	1	4.0 m
1990.3445	176.9	246	1	4.0 m
1991.2500	170	234	0.6	Hipparcos
1991.3903	173.4	234	1	4.0 m
1991.5575	174	240	0.4	2.1 m
1991.5602	174	260	0.4	2.1 m
1991.7124	173.3	226	1	4.0 m
1992.4497	171.7	214	1	4.0 m
1992.6961	164	190	0.4	2.1 m
1994.7079	159.9	192	1	3.8 m
1995.4398	152.5	169	0.6	2.5 m
1995.7675	154.2	177	0.3	2.5 m
1996.5320	145.8	149	0.3	2.5 m
2003.6365	236.3	152	1	3.5 m
2005.7948	218	183	0.6	Direct CFHT
2006.1947	215.8	182	1	4.0 m
2007.3306	212.4	210	1	3.5 m
2007.4927	212.0	212	1	6.0 m
2008.4901	207.8	231	1	6.0 m
2009.2662	204.2	247.5	1	4.0 m

**Notes.** <sup>a</sup> P.A. denotes the position angle and  $\rho$  the angular distance between the central pair (1+2) and the third component. Estimated weight factors  $w$  and uncertainties  $\sigma_{\text{sky}} = 0.005 \text{ arcsec}/w$  correspond to the sizes of telescopes and techniques, which were used to acquire these measurements (1991.25 and 2005 measurements result from direct imaging).

point shifted by 6754 epochs:

$$\text{Pri.Min.} = 2433490.483 + 1^d 1828688 \times E. \quad (1)$$

In the analysis below, when we compare minima timings to our simulations, the period and base minimum are treated as adjustable variables and may therefore differ from the values presented here.

### 2.3. Radial Velocities

We use radial-velocity (RV) data from Tomkin (1992), Table 4, who measured sharp spectral lines in the 5580–5610 Å region and attributed them to the third component. The values of  $v_{\text{rad}3}$  range from  $-13$  to  $-9 \text{ km s}^{-1}$ . One more measurement exists (Worek 1996), which confirms the values given by Tomkin.

The uncertainties of the RV data  $\sigma_{\text{rv}} = 2 \text{ km s}^{-1}$  were estimated from a scatter of the RV measurements close in time. We also checked for possible blends with nearby faint lines—we computed a synthetic spectrum with the same resolution as Tomkin (1992) and fitted the lines in question by a Gaussian function. The observed width of the sharp lines is  $\Delta\lambda \simeq 1 \text{ Å}$ . If we fit them by a Gaussian function, assuming the broadening is mostly caused by a rotational Doppler effect, we can estimate rotational velocity about  $v_{\text{rot}3} = (20 \pm 5) \text{ km s}^{-1}$ .

Wide lines in the V505 Sgr spectrum are attributed to the components of the eclipsing pair (1+2). The binary is tight and in all likelihood rotates synchronously; thus the corresponding rotational Doppler broadening is large ( $v_{\text{rot}1+2} = (100 \pm 10) \text{ km s}^{-1}$ ). The systemic RV of the (1+2) body is  $v_{\text{rad}1+2} = (1.9 \pm 1.4) \text{ km s}^{-1}$ .

**Table 2**  
Minima Timings for the Eclipsing Binary (1+2) in V505 Sgr<sup>a</sup>

HJD – 2400000	Epoch	$O - C$ (d)	$\sigma_{\text{lite}}$ (d)	Source
48432.4871	12632.0	+0.0054	0.0007	R.-L.
48501.0981	12690.0	+0.0100	0.0021	Chochol
48858.3253	12992.0	+0.0109	0.0007	Müyesseroglu
51000.4948	14803.0	+0.0049	0.0007	Ibanoglu
51051.3578	14846.0	+0.0046	0.0007	"
51057.2724	14851.0	+0.0048	0.0007	"
51064.3692	14857.0	+0.0044	0.0007	"
52754.6756	16286.0	-0.0087	0.0007	Chochol
52843.3891	16361.0	-0.0103	0.0007	"
53263.3029	16716.0	-0.0150	0.0007	"
53525.8969	16938.0	-0.0178	0.0007	Cook
53626.4399	17023.0	-0.0187	0.0007	Chochol
54267.5469	17565.0	-0.0266	0.0007	Zasche
54267.5472	17565.0	-0.0263	0.0007	"
54648.4260	17887.0	-0.0313	0.0005	"
54655.5233	17893.0	-0.0312	0.0003	"
54658.4817	17895.5	-0.0299	0.0005	"
54706.3869	17936.0	-0.0309	0.0002	"
55027.5302	18207.5	-0.0365	0.0018	Uhlář
55049.4152	18226.0	-0.0346	0.0002	"
55062.4266	18237.0	-0.0347	0.0011	Šmelcer
55068.3400	18242.0	-0.0357	0.0011	Uhlář

**Notes.** <sup>a</sup> Epoch and  $O - C$  were calculated using the ephemeris Pri.Min. =  $2433490.483 + 1^d 1828688 \times E$ .  $\sigma_{\text{lite}}$  denotes the assumed standard uncertainty of the minimum determination. Only newer minima after Chambliss et al. (1993) are listed. The last four measurements are new.

**References.** Rovithis-Livaniou & Rovithis 1992; Müyesseroglu et al. 1996; Ibanoglu et al. 2000; Cook et al. 2005; Chochol et al. 2006; and Zasche et al. 2009.

**Table 3**  
Free Parameters of Our Dynamical Four-body Model

No.	Parameter	Brief Description
1.	$d$	Distance between the Earth and V505 Sgr barycenter, in pc
2.	$m_3$	Mass of the third body, in $M_\odot$
3.	$z_{h3}$	Position, (1+2)-centric, epoch $T_0$ , in AU
4.	$v_{xh3}$	Velocities, (1+2)-centric, epoch $T_0$ , in AU d $^{-1}$
5.	$v_{yh3}$	
6.	$v_{zh3}$	
7.	$m_4$	Mass of the fourth body, in $M_\odot$
8.	$x_{h4}$	Positions, (1+2)-centric, epoch $T_0$ , in AU
9.	$y_{h4}$	
10.	$z_{h4}$	
11.	$v_{xh4}$	Velocities, (1+2)-centric, epoch $T_0$ , AU d $^{-1}$
12.	$v_{yh4}$	
13.	$v_{zh4}$	

### 3. NUMERICAL INTEGRATOR AND $\chi^2$ METRIC

In order to model orbital evolution of the multiple-star system V505 Sgr, namely mutual gravitational interactions of all bodies, we use a Bulirsch–Stöer (BS)  $N$ -body numerical integrator from the SWIFT package (Levison & Duncan 1994).

Our method is quite general—we can model classical Keplerian orbits, of course, but also non-Keplerian ones (involving three-body interactions). We are able to search for both bound (elliptical) and unbound (hyperbolic) trajectories. Free parameters of our model are listed in Table 3. Hereinafter, we strictly denote individual bodies by numbers: 1, 2 (Algol-type pair), 3 (resolved third component), and 4 to avoid any confusion.

Fixed (assumed) parameters are listed in Table 4. Masses of the first three components are well constrained by photometry

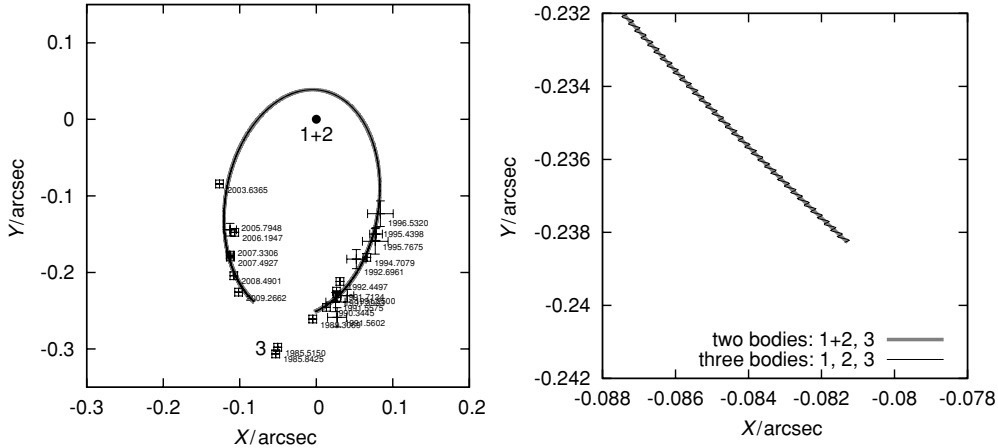


**Figure 1.** Comparison of two third-body trajectories, computed for three-body (1, 2, 3) and two-body (1+2, 3) configurations. Left: an overview of the trajectories in a 1-centric frame. Right: a detail of the small part of the trajectory, where the difference is visible. Error bars denote speckle-interferometry observations.

**Table 4**  
Fixed (Assumed) Parameters of Our Model

No.	Parameter	Brief Description
14.	$m_{1+2} = 3.4 M_\odot$	Mass of the (1+2) body
16.	$x_{h1+2} = 0 \text{ AU}$	Positions of the (1+2) body,
17.	$y_{h1+2} = 0$	(1+2)-centric
18.	$z_{h1+2} = 0$	
19.	$v_{xh1+2} = 0 \text{ AU d}^{-1}$	Velocities
20.	$v_{yh1+2} = 0$	
21.	$v_{zh1+2} = 0$	
22.	$x_{h3}$	Positions of the third body,
23.	$y_{h3}$	(1+2)-centric, in AU
24.	$T_0 = 2446282.24375 \text{ JD}$ (or 2447607.5185)	UTC time corresponding to initial conditions

and spectroscopy:  $m_1 = (2.20 \pm 0.09) M_\odot$ ,  $m_2 = (1.15 \pm 0.05) M_\odot$ ,  $m_3 = (1.2 \pm 0.1) M_\odot$  (Chambliss et al. 1993; Tomkin 1992). We take  $m_3$  as a free parameter, though, because of larger relative uncertainty. When we test three-body configurations, we have simply  $m_4 = 0$ .

First, it is often useful to adopt a simplification: first and second bodies can be regarded as a single (1+2) body in our dynamical model. The central pair (1+2) is so compact ( $a = 0.033 \text{ AU}$ ) and the distance of other components so large that it behaves like a single body; its equivalent  $J_2$  gravitational moment is negligible. Indeed, at distance  $r = 10 \text{ AU}$ ,

$$J_2 \simeq \frac{1}{2} \left( \frac{a}{r} \right)^2 \frac{m_1 m_2}{(m_1 + m_2)^2} \simeq 10^{-6}. \quad (2)$$

This can be confirmed easily by a direct numerical integration. The difference between trajectories computed for three-body (1, 2, 3) and two-body (1+2, 3) configurations is insignificant and always smaller than observational uncertainties (see Figure 1).

We also make use of the following two constraints: (1) initial positions  $x_{h3}$ ,  $y_{h3}$ , and zero time  $T_0$  of the third body correspond to a selected speckle-interferometry datum (e.g., the mean of the first two points, or to the third point) (2) third-body initial velocity components are almost tangent to the observed interferometric trajectory in the  $(x, y)$  plane.

Initial conditions of the integration are specified in an arbitrary (usually 1+2-centric) frame. We then perform a transformation to a barycentric frame. The numerical integration runs in the barycentric Cartesian frame, where  $x, y$  axes correspond to

the sky plane, the  $z$  axis is oriented from the observer toward the system. We use AU, AU day $^{-1}$  units for positions and velocities.

We integrate the system forward for 10,000 days and backward (i.e., with opposite sign of initial velocities) for 20,000 days in order to cover the observational time span. The time step used is  $\Delta t = 10$  days and the precision parameter of the BS integrator is  $\epsilon = 10^{-8}$ . Finally, we transform the output back to the (1+2)-centric frame and linearly interpolate the output data to the exact times of observations.

In order to compare the observations to our model, we constructed a  $\chi^2$  metric as follows:

$$\chi^2 = \chi_{\text{sky}}^2 + \chi_{\text{lite}}^2 + \chi_{\text{rv}}^2, \quad (3)$$

where

$$\chi_{\text{sky}}^2 = \sum_{i=1}^{N_{\text{sky}}} \frac{(x'_{h3} - x_{h3}[i])^2 + (y'_{h3} - y_{h3}[i])^2}{\sigma_{\text{sky}}^2[i]}. \quad (4)$$

We denote  $x'_{h3}$ ,  $y'_{h3}$  (1+2)-centric coordinates of the third body calculated from our model, which were linearly interpolated to the times  $t_{\text{sky}}[i]$  of observations  $x_{h3}[i]$ ,  $y_{h3}[i]$ . Distance  $d$  is used to convert angular coordinates to AU. Second,

$$\chi_{\text{lite}}^2 = \sum_{i=1}^{N_{\text{lite}}} \frac{(z'_{b1+2} - z_{b1+2}[i])^2}{\sigma_{\text{lite}}^2[i]}, \quad (5)$$

where  $z'_{b1+2}$  are barycentric coordinates of the (1+2) body computed from our model and interpolated to the times  $t_{\text{lite}}[i]$  of observations  $z_{b1+2}[i]$ . In order to convert  $O - C$  values from Table 2 to AU, we use a simple formula:  $z_{b1+2} = [O - C]_{\text{days}} \cdot 86,400 \text{ s} \cdot c$ , where  $c$  denotes the speed of light. Because of freedom in the period determination and freedom in the selection of initial velocities, we have to detrend the light-time effect data (by two least-square fits of  $z'_{b1+2}(t)$  and  $z_{b1+2}(t)$ ). Finally,

$$\chi_{\text{rv}}^2 = \sum_{i=1}^{N_{\text{rv}}} \frac{(v'_{zh3} - v_{zh3}[i])^2}{\sigma_{\text{rv}}^2[i]}, \quad (6)$$

where we again interpolate our model to the times  $t_{\text{rv}}[i]$ . Note that in case of a four-body configuration we will attribute the velocities to the fourth body and change this metric correspondingly (see below).

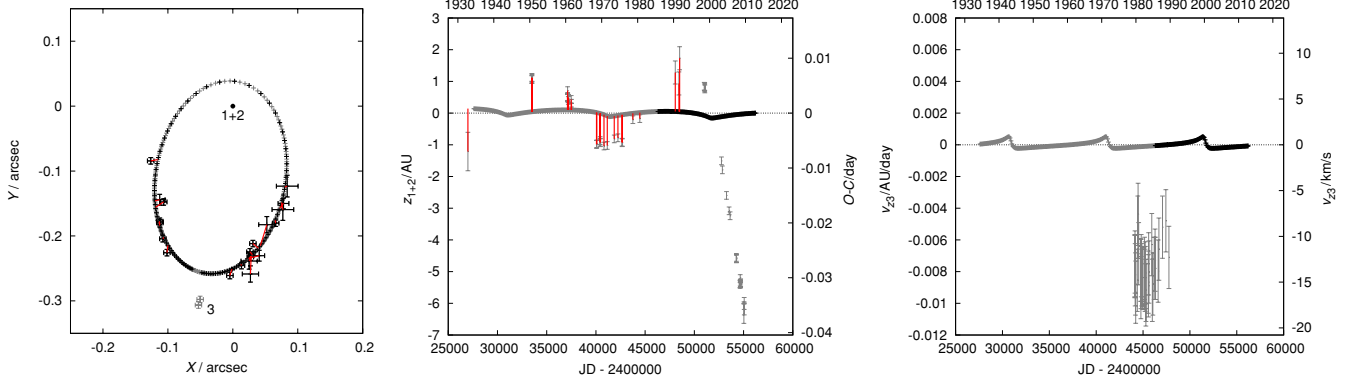


**Figure 2.** Best-fit solution for the trajectory of the third body, which corresponds to speckle-interferometry data (but excluding 1985 measurements). Neither light-time effect nor RVs were fitted in this case. Left panel: trajectory of the third body in the sky-plane angular coordinates ( $X, Y$ ), observations are denoted by error bars and our simulated data by small crosses, red lines represent the residuals. Middle panel: minima timings ( $O - C$ ) of the (1+2) eclipsing binary vs. time ( $JD - 2400000$ ). Right panel: RV  $v_{z3}$  of the third body vs. time. Parameters of the third body are  $m_3 = 1.17 M_\odot$ ,  $x_{h3} = -0.15$  AU,  $y_{h3} = -25.9$  AU,  $z_{h3} = -0.63$  AU,  $v_{xh3} = 0.0037$  AU d $^{-1}$ ,  $v_{yh3} = 0.0017$  AU d $^{-1}$ ,  $v_{zh3} = 0.0000$  AU d $^{-1}$  for  $T_0 = 2447607.5185$  JD. The inclination of the orbit is very low in this case ( $I = 1^\circ.5$ ). The resulting  $\chi^2_{\text{sky}} = 52$ , with the number of data points  $N_{\text{sky}} = 20$ . Note there is a strong disagreement of this Keplerian orbit with both  $O - C$  data and RVs (total  $\chi^2 = 1700$ ,  $N = 90$ ).

(A color version of this figure is available in the online journal.)

Optionally, we can add an *artificial* function to  $\chi^2$  in order to constrain the mass  $m_4$  within reasonable limits, e.g.,

$$\chi^2_{m_4} = \left[ \left( m_4 - \frac{m_{4\min} + m_{4\max}}{2} \right) \cdot \frac{2}{m_{4\max} - m_{4\min}} \right]^{100}, \quad (7)$$

with  $m_{4\min} = 0.1 M_\odot$ ,  $m_{4\max} = 1.2 M_\odot$ . The upper limit follows from the fact that no other bright star is observed in the vicinity of V505 Sgr.

A similar expression can be used to constrain the absolute value of velocity  $v_4$  (e.g., to be smaller than the escape velocity from the system, otherwise, we often obtain hyperbolic velocities).

Occasionally, we use a different metric instead of Equation (3):

$$\chi^2 = w_{\text{sky}} \chi^2_{\text{sky}} + w_{\text{lite}} \chi^2_{\text{lite}} + w_{\text{rv}} \chi^2_{\text{rv}}, \quad (8)$$

with weights  $w_{\text{sky}} \geqslant w_{\text{lite}}, w_{\text{rv}}$ , in order to fit the interferometric trajectory better. There are only five points after the periastron passage, which would otherwise have too low statistical significance compared to a lot of light-time data.

What can we expect about the 13 dimensional function  $\chi^2(d, m_3, z_{h3}, \dots, v_{zh4})$ ? It will surely have many local minima, which would be statistically almost equivalent. (One can shoot the fourth body from a slightly different position with a slightly different velocity to get almost the same result.) The problem is degenerate in this sense. Clearly, there are strong correlations, e.g., between the mass  $m_4$  and the minimal distance of a close encounter (and consequently initial positions/velocities of the fourth body). Minimization of the  $\chi^2$  function is thus a difficult task.

We use a simplex algorithm (Press et al. 1997) to save computational resources and to find local minima. However, it is not our goal to find a global minimum of  $\chi^2$ , because of the degeneracy and the immense size of the parameter space. We anyway do not expect a deep, statistically significant global minimum. Instead, we will choose a set of starting points for the fourth body and look for a subset of *allowed* solutions.

On the other hand, in the case we test a three-body configuration only, the problem is much simpler: the six-dimensional  $\chi^2(d, m_3, z_{h3}, v_{xh3}, v_{yh3}, v_{zh3})$  is well behaved and we may expect to find a unique solution (and its uncertainty).

## 4. RESULTS

In the following subsections, we consider and analyze several hypotheses about the nature of the V505 Sgr system.

1. There are three bodies only in V505 Sgr.
2. The third body directly perturbs the central pair.
3. A steady mass transfer causes minima timing variations.
4. There is modulation of mass transfer by the third body.
5. A sudden mass transfer occurred around 2000.
6. Applegate's mechanism is operating.
7. A fourth body is present (either on a bound or hyperbolic orbit).

### 4.1. The Third Body Alone on a Keplerian Orbit

At first, let us test a standard “null” hypothesis, i.e., only a third body exists ( $m_4 = 0$ ). It is possible to fit speckle data *alone* ( $w_{\text{lite}} = w_{\text{rv}} = 0$ ) by an elliptical orbit with a  $(29 \pm 1)$  year period, especially, if we assume the first two 1985 measurements are erroneous (offset by 50 mas; see Figure 2, left). The  $\chi^2_{\text{sky}} = 50$  for this fit and the respective number of data points is  $N_{\text{sky}} = 20$  (though ideally,  $\chi^2$  should be comparable to  $N$ ).

Note the  $\chi^2_{\text{sky}}$  would be much higher, if we include the 1985 measurements:  $\chi^2_{\text{sky}} = 210$ ,  $N_{\text{sky}} = 22$ . It means, if these two measurements are not systematic errors, the 29 year Keplerian orbit is essentially excluded! The two respective measurements were obtained by two *different* telescopes during two different nights (see McAlister et al. 1987a, 1987b). We checked measurements of another 34 stars in these publications, observed with the *same* telescope and during the same night as V505 Sgr, and we have found no indication of a wrong plate scale—all measurements lie on Keplerian ellipses within usual observational uncertainties (5 mas). We thus believe the 1985 measurements are *not* erroneous and they should be included in the  $\chi^2$  metric.

Without additional (non-positional) data it is not possible to distinguish between different inclinations—there are equivalent low- $I$  and high- $I$  solutions with almost the same  $\chi^2 \simeq 50$ . Nevertheless, *every* inclined orbit of the third body has to cause a corresponding light-time effect, otherwise must be considered wrong! Even a slight  $I \gtrsim 2^\circ$  inclination would easily be

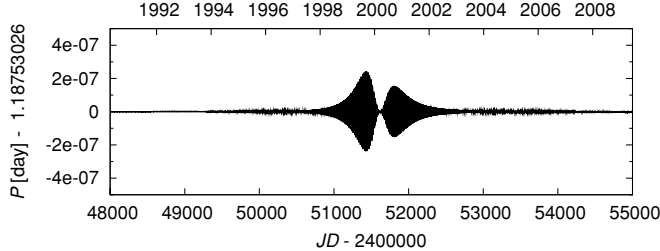


**Figure 3.** Simulated osculating orbital period  $P$  of the central binary (bodies 1 and 2), perturbed by the third body. The periastron passage occurred in 2000 and the corresponding change of period is  $\Delta P \lesssim 10^{-7}$  days. The observed values of  $|\Delta P| \simeq 10^{-5}$  days are much larger than in this simulation.

detectable in the light-time effect data (see Figure 2, middle). A period analysis of the  $O-C$  data (with Period04 program; Lenz 2008) also does not show a prominent 29 year period. On the other hand, there is a clear signal at  $P = 39$  years, with an amplitude of the peak  $A = 0.0092$  days.

If we assume the  $O-C$  data are indeed caused by a light-time effect, there is a strong disagreement of the 29 year Keplerian orbit with the light-time effect data (and also with RVs), even prior to 2000! If we try to fit the whole orbit and light-time effect data *together*, we would have  $\chi^2_{\text{sky}} = 107$  and  $N_{\text{sky}} = 20$ , i.e., such an orbit is excluded with a high significance. There are also clear systematic departures between the observed interferometric data and calculated Keplerian orbit.

The only possibility is that the inclination of the third-body orbit is almost zero  $I \lesssim 2^\circ$ , so we do not see any light-time effect at all. The observed  $O-C$  variations then must be caused by an entirely different phenomenon (see Sections 4.2–4.6 for a detailed discussion).

Nevertheless, there still remains a strong disagreement with the observed high RVs  $v_{\text{rad3}} \simeq 10 \text{ km s}^{-1}$ , because a non-inclined orbit should have  $v_{\text{rad3}} \lesssim 1 \text{ km s}^{-1}$ . We have no solution for this problem (unless there is a fourth body present in the system; see Sections 4.7–4.9).

#### 4.2. Direct Perturbation of the 1+2 Orbital Period by the Third Body

One may ask, if the observed variations in minima timings (Table 2), which correspond to the changes of the period of the order  $|\Delta P| \simeq 10^{-5}$  days, could be caused by a *direct* gravitational perturbation of the tight central pair (1, 2) by the orbiting third body. In periastron, the minimum distance is of the order  $\simeq 10 \text{ AU}$ . So as to test this possibility, we use our dynamical model with three bodies 1, 2, and 3 taken separately. A detection of minute changes of the orbital period requires a smaller time step and higher precision of the BS integrator ( $\Delta t = 0.01 \text{ day}$ ,  $\epsilon = 10^{-12}$ ). The resulting osculating orbital period changes during one periastron passage are shown in Figure 3. They are much smaller than  $\Delta P \lesssim 10^{-7}$  days, if we compare values far from periastron, i.e.,  $\sim 2$  years before and after periastron passage. An extremely close encounter (within less than 0.1 AU, which corresponds to 0.001 arcsec) would be needed to change the orbital period of the tight Algol system substantially.

Moreover, *anything* directly connected with the third body should conform to the 39 year period of the minima timings and this, according to Section 4.1, is in conflict with any 29 year Keplerian orbit of the third body.

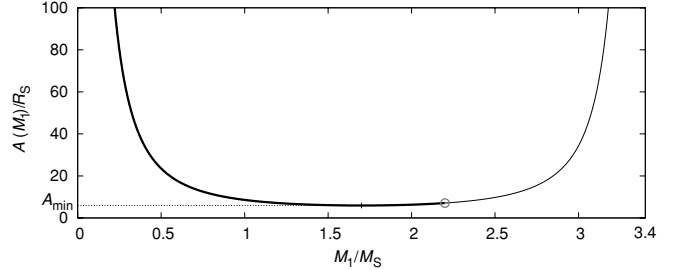


**Figure 4.** Dependence of separation  $A$  of the eclipsing binary on the mass  $M_1$  of the first body, resulting from the conservation of total mass and orbital angular momentum. The thick line denotes past evolution, the circle the current state  $M_1 = 2.2 M_\odot$ , and the thin line the future evolution.

#### 4.3. Effects of Mass Transfer Between 1 and 2

Past photometric and spectroscopic observations confirm that the central pair of V505 Sgr is a classical semi-detached Algol system, with a less-massive secondary filling its Roche lobe (Chambliss et al. 1993). In the case of a conservative mass transfer, the sum of masses is constant,

$$M_1(t) + M_2(t) = K, \quad (9)$$

as well as the orbital angular momentum

$$A(t)M_1^2(t)M_2^2(t) = C, \quad (10)$$

where  $A(t)$  denotes the actual separation of the stars. We can substitute current masses and separation  $A = 7.1 R_\odot$  (Chambliss et al. 1993) into these equations, compute constants  $K$ ,  $C$ , and consequently the dependence  $A(M_1)$  (see also Figure 4),

$$A(M_1) = CM_1^{-2}(K - M_1)^{-2}. \quad (11)$$

A smooth conservative mass transfer should increase the orbital period steadily, since in the V505 Sgr case the mass ratio has been reversed already ( $M_1 > M_2$ ). On the contrary, we observe an abrupt *decrease* of the period  $\Delta P = -1.2 \times 10^{-5}$  days after 2000. We thus conclude a simple mass transfer cannot explain the observer minima timings.

#### 4.4. Modulation of Mass Transfer Between 1 and 2 During the Third-body Encounter

In this section, we test if the third body is capable of changing the Roche potential of the central binary (bodies 1 and 2) in a such a way that the mass transfer rate  $dM/dt$  (and consequently  $dP/dt$ ) changes by a substantial amount. We add a third-body term to the Roche potential:

$$\Omega(x, y, z) = \frac{1}{r_1} + \frac{q}{r_2} + \frac{1}{2}(1+q)r_3^2 + \frac{q_{3\text{rd}}}{r_{3\text{rd}}}, \quad (12)$$

where  $q = M_2/M_1$  denotes the mass ratio and similarly  $q_{3\text{rd}} = M_3/M_1$ . We see immediately, that relative change of the potential due to the third body at distance  $r_{3\text{rd}} \simeq 10 \text{ AU}$  is  $\delta\Omega/\Omega \simeq 10^{-13}$ . We do not find it likely that such a minuscule perturbation of the potential, and thus the related tidal acceleration, could produce significant effects. Consequently, we cannot explain minima timing variations by the modulation of mass transfer. Finally, as in Section 4.2, this effect would also be in conflict with a 29 year Keplerian orbit of the third body.

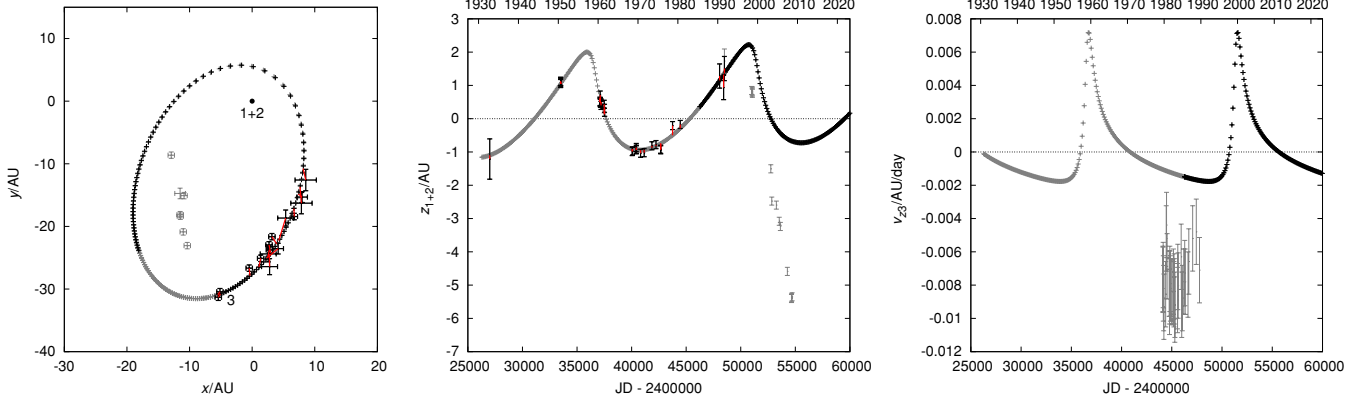


**Figure 5.** Best-fit solution for the orbit of the third body and the light-time effect before 2000:  $d = 102$  pc,  $m_3 = 1.2 M_{\odot}$ ,  $z_{h3} = 4.0$  AU,  $v_{xh3} = 0.0036$  AU day $^{-1}$ ,  $v_{yh3} = 0.0013$  AU day $^{-1}$ ,  $v_{zh3} = -0.0015$  AU day $^{-1}$  for  $T_0 = 2446282.24375$  JD. The resulting  $\chi^2 = 88$ , with the total number of data points  $N = 46$ . The red lines denote differences between observed and calculated data. Radial velocities were not fitted in this case; they are shown for comparison only.

(A color version of this figure is available in the online journal.)

#### 4.5. A Sudden Mass Transfer of Biermann & Hall (1973)

According to Biermann & Hall (1973) a sudden mass transfer between the Algol components may result in a temporary decrease of the orbital period, even though mass is flowing from the lighter component to the more massive one. In our case, we would need  $dM/dt$  as high as  $\simeq 10^{-6} M_{\odot}$  yr $^{-1}$  to explain period changes  $|dP/dt| \simeq 10^{-6}$  days yr $^{-1}$ . Such a mass transfer rate seems to be too large compared to theoretical models (Harmanec 1970),  $dM/dt \gtrsim 10^{-6} M_{\odot}$  yr $^{-1}$  are reached only during a very short interval of time, before the reversal of mass ratio.

Another problem of this scenario is that we observe rather smooth periodic variations of the minima timings before 2000. These do not seem to be entirely compatible with this mechanism, which may be more irregular in time. This phenomenon is also rarely confirmed by independent observations. (It would require a very precise photometry on a long timescale or a spectroscopic confirmation of circumstellar matter.) Today, this mechanism is not generally accepted as a major cause of minima timing variations among Algol-type systems.

#### 4.6. Applegate (1992) Magnetic Mechanism

Applegate (1992) proposed that a gravitational quadrupole coupling of orbit and shape variations of a magnetically active subgiant (second component) can result in variations of the orbital period and hence minima timings. In this scenario, the observed 39 year period would correspond to the period of the magnetic dynamo.

The second (G5 IV) star rotates quickly (1.2 d); it has a convective envelope in this evolutionary stage and, presumably, there is a differential rotation and operating dynamo, which can result in a sufficiently strong magnetic field ( $10^4$  G), necessary for Applegate's mechanism to work. Period changes of the order  $\Delta P/P \simeq 10^{-5}$  should also correspond to changes of the luminosity  $\Delta L_2/L_2 = 0.1$ , in phase with minima timings. Unfortunately, we are not able to confirm this by our photometry (0.01 mag precision over tens of years would be required).

In principle, this mechanism can explain minima timing variations, but it is not clear, why there is an abrupt change after 2000. An independent confirmation is rare and difficult. One of the possibilities might be a spectroscopic observation of magnetically active lines (Ca II H and K or Mg II). This scenario also does not provide any solution for the observed large RVs.

#### 4.7. Distance, Mass, and the Third-body Orbit (Prior to 2000)

Hereinafter, we assume minima timing variations are caused mainly by the light-time effect due to the orbiting third body. Because the orbit of the third body prior the periastron passage in 2000 seems unperturbed, we first determine the optimal distance  $d$  of the system, third-body mass  $m_3$ , and orbit ( $z_{h3}$ ,  $v_{xh3}$ ,  $v_{yh3}$ ,  $v_{zh3}$ ). We use only the observational data older than 2000 for this purpose.

We compute  $\chi^2$  values for the following set of initial conditions (we do not use a simplex here):  $d \in (95, 105)$  pc,  $\Delta d = 1$  pc,  $m_3 \in (1.1, 1.3) M_{\odot}$ ,  $\Delta m_3 = 0.1 M_{\odot}$ ,  $z_{h3} \in (2.0, 8.0)$  AU,  $\Delta z_{h3} = 1.0$  AU,  $v_{xh3} \in (0.0033, 0.0040)$  AU day $^{-1}$ ,  $v_{yh3} \in (0.0008, 0.0016)$  AU day $^{-1}$ ,  $v_{zh3} \in (-0.0018, 0.0012)$  AU day $^{-1}$ ,  $\Delta v_{xh3} = \Delta v_{yh3} = \Delta v_{zh3} = 0.0001$  AU day $^{-1}$ .

The best-fit solution is displayed in Figure 5. The orbital period of the third body is  $P = (39 \pm 2)$  years. The resulting distance  $d = (102 \pm 5)$  pc. This solution is very similar to that in Mayer (1997). The parallactic distance of V505 Sgr given by Hipparcos ( $\pi = (8.40 \pm 0.57)$  mas,  $d = 111\text{--}128$  pc, cf., van Leeuwen 2007) is offset and even the error intervals do not overlap.

Note that the RVs of the order  $-10$  km s $^{-1}$  measured by Tomkin (1992) cannot be attributed to the third body, whose orbital velocity should be much smaller ( $(-2.5 \pm 0.5)$  km s $^{-1}$ ) according to interferometric and light-time effect data. Consequently, we do not fit the velocities in this case ( $w_{rv} = 0$ ); we are going to attribute them to the fourth body (in Section 4.8).

Finally, it is important to mention that our solution does not depend on the two ("offset") 1985 speckle measurements at all! We can exclude them completely from our considerations and the result would be the same. Our only assumption was that minima timing variations are caused by the light-time effect and this enforces the orbital period of  $P \simeq 39$  years. (But coincidentally, both 1985 measurements fit perfectly this longer-period orbit.)

#### 4.8. Encounter with a Fourth Body (a $\chi^2$ Map)

We next fix initial conditions of the third body according to the results in Section 4.7 and model a perturbation by a fourth body under different geometries.

The free parameters of the model are  $m_4$ ,  $x_{h4}$ ,  $y_{h4}$ ,  $z_{h4}$ ,  $v_{xh4}$ ,  $v_{yh4}$ ,  $v_{zh4}$ . We include RV data, but we assume the spectral lines (and corresponding velocities) belong to the fourth

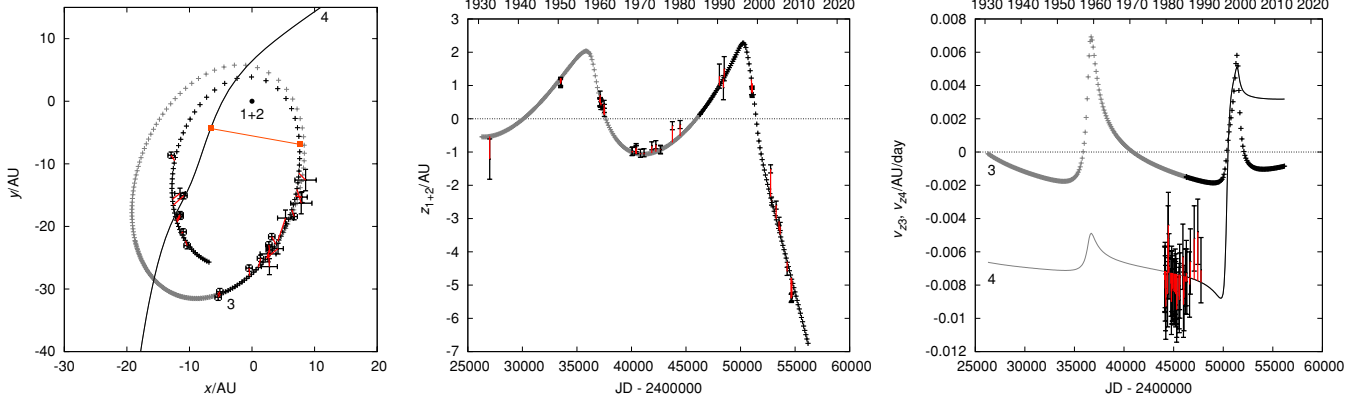


**Figure 6.** Best-fit solution for the trajectory of the fourth body, which best explains the observed trajectory of the third body, light-time effect, and RVs:  $m_4 = 0.8 M_\odot$ ,  $x_{h4} = 45.0 \text{ AU}$ ,  $y_{h4} = 39.5 \text{ AU}$ ,  $z_{h4} = 28.0 \text{ AU}$ ,  $v_{xh4} = -0.0105 \text{ AU day}^{-1}$ ,  $v_{yh4} = -0.008 \text{ AU day}^{-1}$ ,  $v_{zh4} = -0.0075 \text{ AU day}^{-1}$ . The resulting  $\chi^2 = 331$ , with the total number of data points  $N = 102$ . The motion of the fourth body captured in the left panel spans from 1994 to 2003. The squares connected by a straight line indicate the closest encounter between the third and fourth bodies.

(A color version of this figure is available in the online journal.)

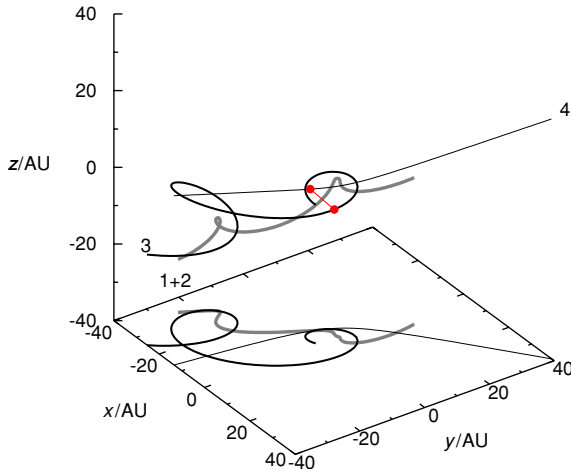


**Figure 7.** Orbits of bodies (1+2), 3, 4 in a barycentric frame and their projection to the plane ( $z = -40 \text{ AU}$ ).

(A color version of this figure is available in the online journal.)

body. Note that there might be a problem with too low luminosity and thus too weak spectral lines of the fourth body, in case it has low mass. We discuss this possible inconsistency in detail in Section 4.11. We scan the following limited set of initial conditions (over 8 million trials):  $m_4 \in (0.5, 0.8) M_\odot$ ,  $\Delta m_4 = 0.05 M_\odot$ ,  $x_{h4} \in (38, 45) \text{ AU}$ ,  $\Delta x_{h4} = 1.0 \text{ AU}$ ,  $y_{h4} \in (37, 40) \text{ AU}$ ,  $\Delta y_{h4} = 0.5 \text{ AU}$ ,  $z_{h4} \in (20, 30) \text{ AU}$ ,  $\Delta z_{h4} = 1.0 \text{ AU}$ ,  $v_{xh4} \in (-0.011, -0.005) \text{ AU day}^{-1}$ ,  $v_{yh4} \in (-0.010, -0.005) \text{ AU day}^{-1}$ ,  $v_{zh4} \in (-0.012, -0.006) \text{ AU day}^{-1}$ ,  $\Delta v_{xh4} = \Delta v_{yh4} = \Delta v_{zh4} = 0.0005 \text{ AU day}^{-1}$ .

A comparison of the best-fit solution with observational data is displayed in Figure 6. We use a modified metric, Equation (8), with  $w_{\text{sky}} = 10$ ,  $w_{\text{lite}} = w_{\text{rv}} = 1$ . The respective trajectories of the bodies are shown in Figure 7. Note, however, that according to the  $\chi^2$  map (Figure 8) there are many local minima, which cannot be distinguished from a statistical point of view, because the values of  $\chi^2$  differ only little ( $\chi^2 \in [284, 325]$ ). The corresponding  $\chi^2$  probabilities  $Q(\chi^2 | N)$  that the observed value of  $\chi^2 = 340$  (for a given number of degrees of freedom  $N = 105$ ) is that large by chance even for a correct model are too low (essentially zero). It may also indicate that real uncertainties might be a bit larger (by a factor of 2) than the values estimated

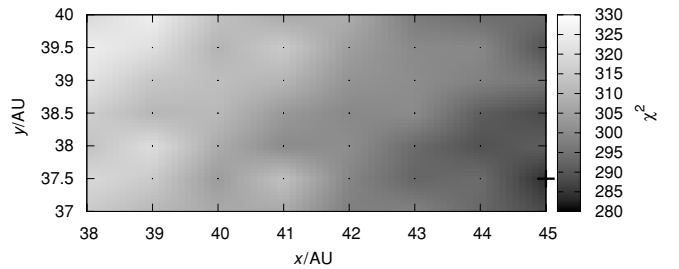


**Figure 8.** Minima of the seven-dimensional function  $\chi^2(m_4, x_{h4}, y_{h4}, z_{h4}, v_{xh4}, v_{yh4}, v_{zh4})$  at given positions  $(x_{h4}, y_{h4})$ . The minimum is taken over remaining free parameters  $m_4, z_{h4}, v_{xh4}, v_{yh4}, v_{zh4}$ . Cross is an overall minimum and black dots represent computed points.

by us. Nevertheless, we will find better solutions using a simplex method (in Section 4.9).

#### 4.9. Encounter with a Fourth Body (Different Geometry, Simplex)

We selected a different set of initial conditions for the following modeling. They serve as starting points for the simplex algorithm:  $m_4 = 0.5 M_\odot$ ,  $x_{h4} \in (-100, -10) \text{ AU}$ ,  $y_{h4} \in (-50.1, -0.1) \text{ AU}$ ,  $z_{h4} \in (0, 50) \text{ AU}$ ,  $\Delta x_{h4} = \Delta y_{h4} = \Delta z_{h4} = 5.0 \text{ AU}$ ,  $v_{xh4} \in (0.005, 0.015) \text{ AU day}^{-1}$ ,  $\Delta v_{xh4} = 0.001 \text{ AU day}^{-1}$ ,  $v_{yh4} \in (0, 0.01) \text{ AU day}^{-1}$ ,  $\Delta v_{yh4} = 0.002 \text{ AU day}^{-1}$ ,  $v_{zh4} \in (-0.007, 0) \text{ AU day}^{-1}$ ,  $\Delta v_{zh4} = 0.001 \text{ AU day}^{-1}$ . The total number of trials reaches  $10^6$ .

We reject RV constraints ( $w_{\text{rv}} = 0$ ), although we can find a lot of allowed solutions with velocities in the correct range ( $v_{zh4} \doteq -0.008 \text{ AU day}^{-1}$ ). On the other hand, we use a mass limit according to Equation (7). An example of a typical good fit is shown in Figure 9. We selected one with mass around  $m_4 = 0.6 M_\odot$ ; the corresponding  $\chi^2 = 168$ ,  $N = 73$ , and probability  $Q(\chi^2 | N) \simeq 10^{-9}$ , still too low. This solution can be further improved by a 15 dimensional simplex (i.e., with all parameters of the third-body free) to reach  $\chi^2$  as low as 130 and  $Q(\chi^2 | N)$  as high as  $10^{-5}$ .

As before, there are many solutions, which are statistically equivalent. We present allowed solutions in Figure 10 as plots  $\chi^2$  versus a free parameter, with each dot representing one local minimum found by simplex. Prominent concentrations of solutions in these plots can be regarded as an indication of more

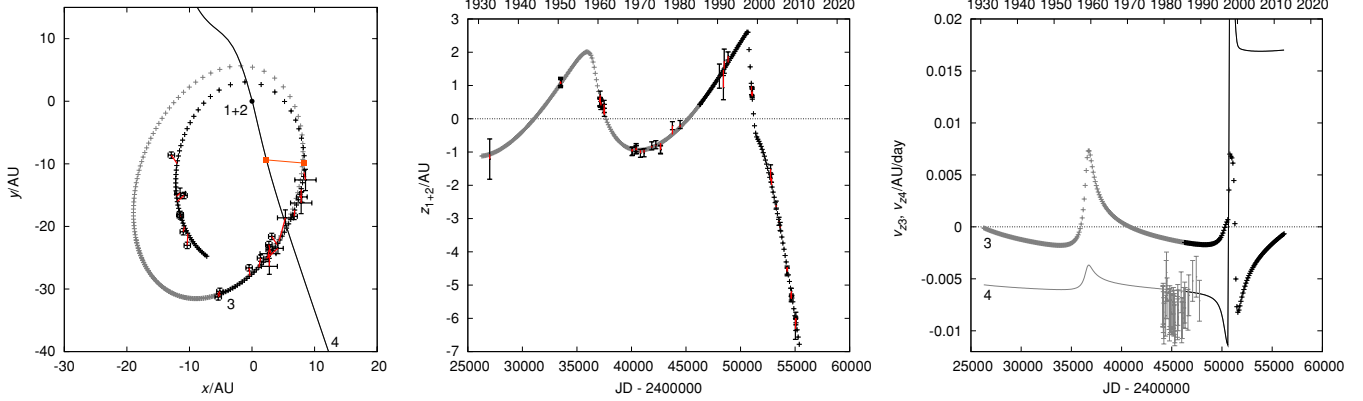


**Figure 9.** Typical solution (out of many) for the trajectory and light-time effect (without RVs):  $m_4 = 0.576 M_{\odot}$ ,  $x_{h4} = 27.912$  AU,  $y_{h4} = -84.809$  AU,  $z_{h4} = 30.482$  AU,  $v_{xh4} = -0.00584$  AU day $^{-1}$ ,  $v_{yh4} = 0.01612$  AU day $^{-1}$ ,  $v_{zh4} = -0.00620$  AU day $^{-1}$ . The corresponding  $\chi^2 = 168$ , with the number of data points  $N = 73$ . This solution can be further improved by a 15 dimensional simplex to reach  $\chi^2$  as low as 130.

(A color version of this figure is available in the online journal.)

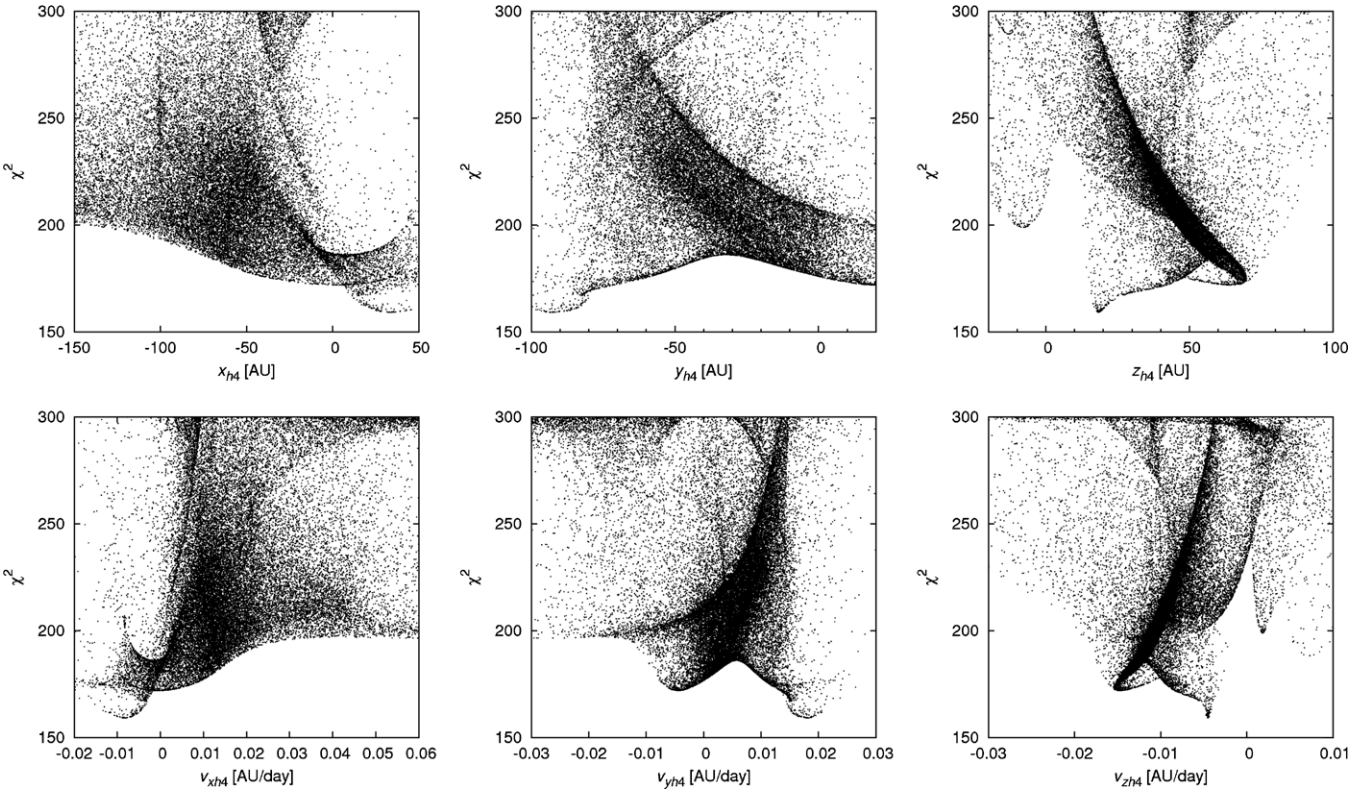


**Figure 10.** Distribution of good solutions ( $\chi^2 < 300$ ) in the space of free parameters:  $x_{h4}$ ,  $y_{h4}$ ,  $z_{h4}$ ,  $v_{xh4}$ ,  $v_{yh4}$ ,  $v_{zh4}$ .

probable solutions. Only minority of trials were successful. Most of them were stopped too early (at high  $\chi^2$ ) due to numerous local minima.

According to the histogram of masses  $m_4$  (Figure 11, left) the values  $m_4 < 0.5 M_{\odot}$  are less probable, and the histogram peaks around  $m_4 = 0.9 M_{\odot}$ . Note the simplex sometimes tends to “drift” to zero or large masses, which leads to artificial peaks at the limits of the allowed interval. The same applies to velocity  $v_4$ .

Histogram of total energies  $E_4$  of the fourth body (Figure 11, middle) shows a strong preference for hyperbolic orbits ( $E_4 > 0$ ), but elliptic orbits ( $E_4 < 0$ ) also exist (with a 1% probability and slightly larger best  $\chi^2 = 199$ ).

The reason for this preference stems from the fact that third-body orbit seems almost unperturbed prior to 2000, so one needs rather a higher-velocity encounter of the fourth body from larger initial distance.

Typical minimum distances between the fourth and third bodies during an encounter are around  $d_{\min 3} \simeq 6$  AU and they are even smaller between the fourth body and the (1+2) body  $d_{\min 1+2} \simeq 1.5$  AU (Figure 11, right). They are of comparable size and consequently a simple impulse approximation, i.e., an instantaneous change of orbital velocity, cannot be used to link the two elliptic orbits of the third body (before and after the perturbation). There are no good solutions (with  $\chi^2 < 300$ ), which would lead to an escape of the third body.

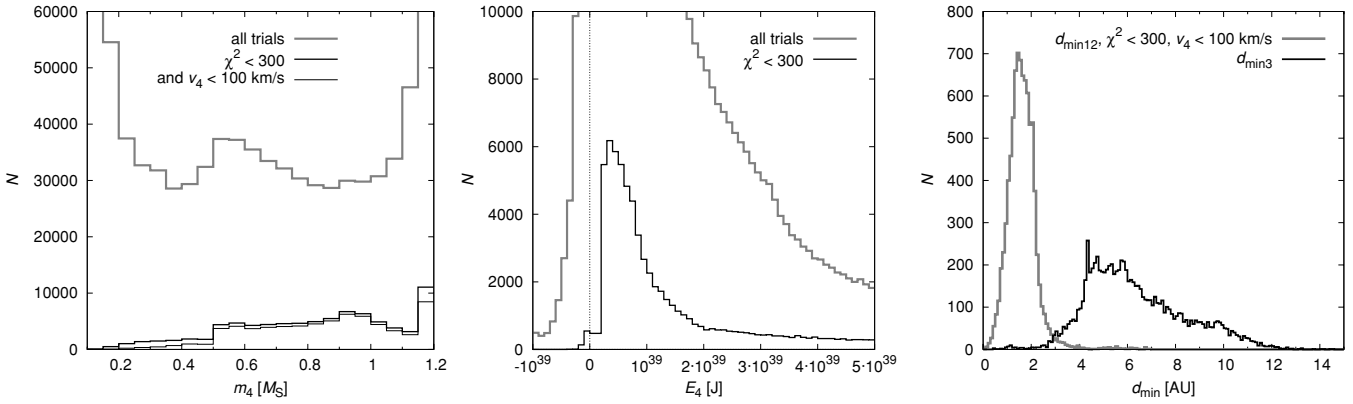


**Figure 11.** Left: histogram of masses  $m_4$  of all trials and good ones (with  $\chi^2 < 300$  and the lower absolute value of velocity  $|v_4| < 100 \text{ km s}^{-1}$ ). Middle: histogram of total energies  $E_4$  of the fourth body at the epoch  $T_0$ . There is a strong preference for hyperbolic orbits ( $E_4 > 0$ ), but one can find approximately 1% of orbits with negative energies. Right: histogram of minimum distances  $d_{\min 1+2}, d_{\min 3}$  of the fourth body from the (1+2) and third body (only good trials are shown). According to these distributions, it is more likely that the fourth body approached the (1+2) body closer than the third body. Median values are  $d_{\min 1+2} = 1.6 \text{ AU}$  and  $d_{\min 3} = 5.9 \text{ AU}$ .

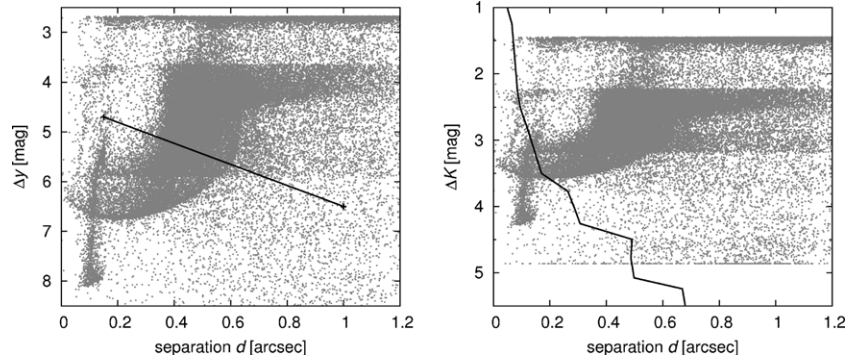


**Figure 12.** Observational limits (black lines) of interferometric measurements (left panel) and the CFHT imaging (right panel). Our solutions from Section 4.9 are plotted as dots. Many of them are well below the observational limits.

#### 4.10. Observational Limits of Interferometry and CFHT Imaging

Postulating an existence of a fourth body, inferred from its gravitational influence on the V505 Sgr system, we should check if this object could have been directly observed in the past.

According to A. Tokovinin (2009, private communication), the limit of recent interferometric measurements can be approximated by a linear dependence of brightness difference  $\Delta y$  in Strömgren  $y$  magnitudes on angular separation  $d$  of the components:  $\Delta y = 4.7 \text{ mag}$  at  $d = 0.15 \text{ arcsec}$  and  $\Delta y = 6.5 \text{ mag}$  at  $d = 1 \text{ arcsec}$  adaptive optics at CFHT can reach even fainter. The limit in the  $K$  band is given by Rucinski et al. (2007), Figure 7, as a nonlinear dependence  $\Delta K(d)$ .

We can easily select solutions from Section 4.9, which fulfill both limits, albeit a lot of them is excluded by the CFHT limit (see Figure 12). Note that we are not able to predict exact magnitudes or positions of the fourth body, because there are still many solutions possible.

Note that there is an object in the USNO-A2.0 catalog, very close to V505 Sgr: 0750-19281506, R.A.<sub>J2000</sub> = 298°277034, decl.<sub>J2000</sub> = -14°603839. This corresponds to an angular separation of 2.6 arcsec and a position angle of 235° with respect to V505 Sgr, at the epoch of observation 1951.574. The magnitudes  $R = 10.9 \text{ mag}$  and  $B = 11.8 \text{ mag}$  are marked as uncertain (since the object is located in the area flooded by light of V505 Sgr). This is an interesting coincidence with "our" fourth body, but we doubt if the source is real. Moreover, if the brightness of the USNO source is correct within

$\pm 1 \text{ mag}$ , it should be well above the observational limits of CFHT.

#### 4.11. Constraints from Spectral Lines Radial-velocity Measurements

In Section 4.8, we tried to attribute the observed high RVs to a hypothetic fourth component. We thus have to ask a question: could the low-mass fourth component be visible in the spectrum?

To this end, we used a grid of synthetic spectra based on Kurucz model atmospheres, which was calculated and provided for general use by J. Kubát (for details of the calculations, cf., e.g., Harmanec et al. 1997). We calculate synthetic spectra for three and four lights (stars) and compare them with the spectrum observed by Tomkin (1992), Figure 2. This spectrum was taken at HJD = 2444862.588, close to the primary eclipse of the central binary, which decreases the luminosity of the first component and thus weak narrow lines of the third (or fourth) component are more prominent.

Modeling of spectra (relative intensities) requires a number of parameters: luminosities, effective temperatures, surface gravity, rotational and RVs. Luminosities of the known components are  $L_1 = 26 L_{\odot}$ ,  $L_2 = 3.8 L_{\odot}$ ,  $L_3 = 2.1 L_{\odot}$ , respectively. The amplitude of the light curve is  $\Delta m = 1.1 \text{ mag}$  (Chambliss et al. 1993). The effective temperatures are approximately (Popper 1980)  $T_{\text{eff}1} \simeq 9000 \text{ K}$  (corresponding to A2 V spectral type),  $T_{\text{eff}2} \simeq 6000 \text{ K}$  (F8 IV to G6–8 IV),  $T_{\text{eff}3} \simeq 6000 \text{ K}$  (F8 V). We assume the following values of the surface gravitational

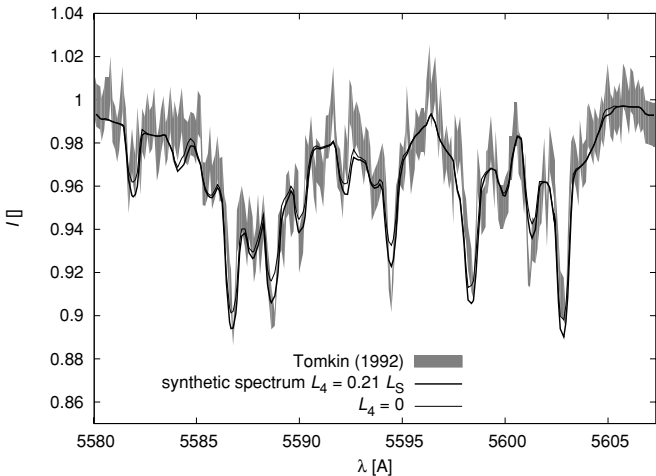


**Figure 13.** Synthetic spectrum with intensity normalized to the continuum for four and three lights (thick and thin lines) and for the temperature of the fourth body equal to 4000 K, compared with the observed spectrum (gray line, whose thickness corresponds to observational uncertainties), taken from Tomkin (1992). The wavelength range, which we fitted, was 5580–5607 Å. The best solution for the luminosity of the fourth body is  $L_4 = 0.22 L_\odot$  (with  $\chi^2 = 465, N = 239$ ) The fit with three lights only is worse, with the  $\chi^2$  value equal to 542. For  $T_4 = 5700$  K, we would have  $L_4 = 0.43 L_\odot$  and  $\chi^2 = 495$ .

acceleration:  $\log g_1 = \log g_2 = 4.0$  (cgs units),  $\log g_3 = 4.5$  (valid for stars close to the main sequence). Rotational velocities of the first and second components, a semi-contact binary with an orbital period of 1.2 days, are synchronized by tidal lock and are of the order  $v_{\text{rot}1} \simeq v_{\text{rot}2} \simeq 100 \text{ km s}^{-1}$ . These are in concert with the observed width of broad spectral lines  $\Delta\lambda = 6 \text{ Å}$ . For the third component, we assume a lower velocity  $v_{\text{rot}3} = 20 \text{ km s}^{-1}$ , usual for late F-type main-sequence stars. This matches the width of sharp lines. Radial velocities of the first and second components are close to zero because of the eclipse proximity ( $v_{\text{rad}1} = v_{\text{rad}2} \doteq 0$ ).

We assume the following reasonable parameters for the fourth component:  $T_4 = 4000$  K or  $5700$  K,  $\log g_4 = 4.0$ ,  $v_{\text{rot}4} = 20 \text{ km s}^{-1}$ . We construct a  $\chi^2$  metric:

$$\chi^2 = \sum_{i=1}^{N_{\text{obs}}} \frac{(I_{\text{obs}}[i] - I')^2}{\sigma_{\text{obs}}[i]^2}, \quad (13)$$

where  $I_{\text{obs}}[i]$  denote observed relative intensities,  $\sigma_{\text{obs}}[i]$  associated uncertainties, and  $I'$  is a sum of synthetic intensities weighted by luminosities:

$$I' = \frac{\sum_{j=1}^4 I'(T_{\text{eff}j}, \log g_j, v_{\text{rot}j}) \cdot L_j}{\sum_{j=1}^4 L_j} \quad (14)$$

and of course Doppler shifted due to RVs ( $\lambda' = \lambda_{\text{obs}}[i](1 - v_{\text{rad}j}/c)$ ) and interpolated to the required wavelengths  $\lambda'$  using Hermite polynomials (Hill 1982). We use a simple eclipse modeling: we decrease  $L_1$  according to the Pogson equation to get the observed total magnitude increase  $\Delta m$ . Errors  $\sigma_{\text{obs}}[i]$  were estimated from the scatter in small continua,  $\sigma = 0.01$ . Artificially small errors  $\sigma = 0.003$  were assigned to the measurements in the cores of the narrow lines, in order to match precisely their depths.

We constructed a simplex algorithm (Press et al. 1997) with the following free parameters:  $L_4, v_{\text{rad}3}, v_{\text{rad}4}$ . Other luminosities and RVs remain fixed. This simplex is well behaved and converges to final values almost regardless of the starting

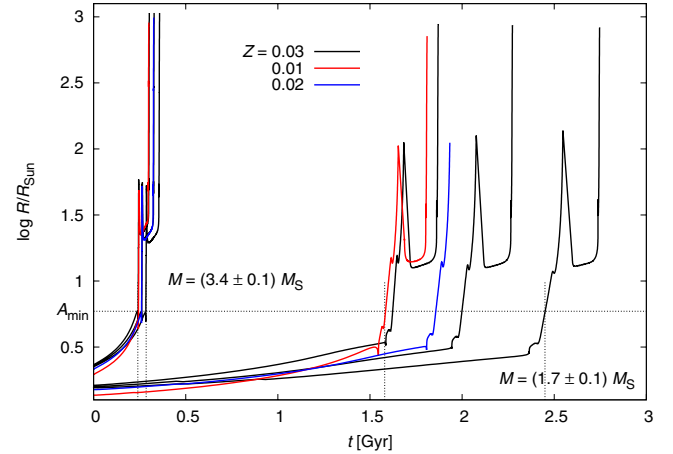


**Figure 14.** Evolution of radii for stars with different masses ( $M = 1.6, 1.7, 1.8$ , and  $3.3, 3.4, 3.5 M_\odot$ ,  $Z = 0.03$ ) and metallicities ( $M = 1.7$  and  $3.4 M_\odot$ ,  $Z = 0.01, 0.02$ ). This computation was performed by the program EZ (Paxton 2004). The upper limit for the age of the second component is then 1.5–2.5 Gyr, while the lower limit is between 0.24 and 0.29 Gyr.

(A color version of this figure is available in the online journal.)

point. There is no reasonable improvement, if we let all eight parameters ( $L_j, v_{\text{rad}j}$ ) to be free.

The result for a selected temperature  $T_4 = 4000$  K is shown in Figure 13. The best fit is for  $L_4 = 0.22 L_\odot$ , and it is marginally better than the fit with three lights only (i.e., with fixed  $L_4 = 0$ ). The luminosity corresponds roughly to the mass  $m_4/M_\odot \propto (L_4/L_\odot)^{1/4} = 0.68$ , which seems reasonable with respect to the results in Section 4.9.

Note that we used  $v_{\text{rot}3} = 20 \text{ km s}^{-1}$  for rotational velocity of the third body. No reasonable solution was found for  $v_{\text{rot}3}$  as high as  $100 \text{ km s}^{-1}$ , which would cause a strong rotational broadening and almost a “disappearance” of spectral lines of the third body. It means that a low-mass fourth body *alone* cannot produce deep sharp lines. We thus suspect, there is a blend of lines in the spectrum observed by Tomkin (1992), which may originate on the third and fourth bodies, with low and high RVs. However, observations with high spectral resolution would be needed to resolve such blending.

#### 4.12. Constraints from the Stellar Evolution of the Eclipsing Binary

To assess the long-term evolution of V505 Sgr, we need some information about the age of the system. An *upper* limit for the age can be estimated easily from masses of stars. The semi-detached central binary (bodies 1 and 2) has a total mass  $(3.4 \pm 0.1) M_\odot$ . In order to evolve into the current stage, when the second *lighter* component fills its Roche lobe, the original mass of the second star had to be at least slightly larger than half of the total mass, i.e.,  $M_2 > 1.7 M_\odot$ . The evolution of radius is shown in Figure 14; we are mainly concerned with the large increase of radius, when the star leaves main sequence. Given the uncertainties of the masses and unknown metallicities, the upper limit for the age is  $(2.0 \pm 0.5)$  Gyr.

In order to find a lower limit, we have to check a minimum separation of the components first (cf. Equation (11) and Figure 4). A minimum separation occurs when  $M_1 = 0.5$  K, in our case  $A_{\min} = (5.9 \pm 0.1) R_\odot$ . This value is larger than the radius of a  $3.4 M_\odot$  star during the whole evolution on the main sequence. Thus, the mass transfer had to start later, in the red giant phase.

The maximum mass of the second star had to be slightly below the total mass, i.e.,  $M_2 < 3.4 M_{\odot}$ . According to the  $R(t)$  dependence (Figure 14), the red giant phase starts at the age of  $(0.26 \pm 0.03)$  Gyr, which could be considered as a *lower* limit for the age of the V505 Sgr system.

## 5. CONCLUSIONS

Generally speaking, we are able to explain the observed orbit of the third body together minima timings and RVs by a low-mass fourth body, which encounters the observed three bodies with a suitable geometry. There is no unique solution, but rather a set of allowed solutions for the trajectory of the hypothetic fourth body. It is quite difficult to find a solution for both speckle-interferometry and light-time effect data. There are a few systematic discrepancies at the  $2\sigma$  level, which cause the likelihood of the hypothesis to be low. Possibly, realistic uncertainties  $\sigma_{\text{sky}}$  are slightly larger (by a factor of 1.5) than the errors estimated by us.

Of course, there are other hypotheses, which do not need a fourth body at all (a sudden mass transfer, Applegate's mechanism, etc.), but none of them provides a unified solution for *all* observational data we have for V505 Sgr.

Further observations of the light-time effect during the next decade can significantly constrain the model. A new determination of the systemic velocity of V505 Sgr may confirm, that the change in the  $O - C$  data after 2000 resulted from an external perturbation. (Tomkin's (1992) value was  $(1.9 \pm 1.4)$  km s $^{-1}$ .) Spectroscopic measurements of the indicative sharp lines would also be very helpful to resolve the problem with radial velocities and relative intensity of spectral lines. These lines can be attributed neither to the third nor to the fourth body alone.

If we indeed observe the V505 Sgr system by chance during the phase of a close encounter with a fourth star, we can imagine several scenarios for its origin:

1. A random passing star approaching V505 Sgr on a hyperbolic orbit. The problem of this scenario is a very low number density of stars. If we take the value  $n_{\star} \simeq 0.073 \text{ pc}^{-3}$  from the solar vicinity (Fernández 2005), the mean velocity with respect to other stars of the order  $v_{\text{rel}} \simeq 10 \text{ km s}^{-1}$  and the required minimum distance of the order  $r_{\text{imp}} \simeq 10^2 \text{ AU}$ , we end up with a mean time between two encounters  $\tau \simeq 1/(n_{\star} v_{\text{rel}} r_{\text{imp}}^2) \simeq 10^{12} \text{ yr}$ , thus an extremely unlikely event.
2. A loosely bound star on a highly eccentric orbit, with the same age as other three components of V505 Sgr. Unfortunately, there is a large number of revolutions and encounters ( $10^2$ – $10^5$ ) over the estimated age of V505 Sgr and the system practically cannot remain stable over this timescale (Valtonen & Mikkola 1991).
3. A more tightly bound star on a lower-eccentricity orbit, which experienced some sort of a late instability, induced by long-term evolution due to galactic tides, distant passing stars, which shifted an initially stable configuration into

an unstable state, e.g., driven by mutual gravitational resonances between components. The problem in this case is that tightly bound orbits of the fourth body are very rare in our simulations, thus seem improbable.

None of the scenarios is satisfactory. Nevertheless, we find the fourth-body hypothesis, the only one which is able to explain all available observations. Clearly, more observations and theoretical effort is needed to better understand the V505 Sagittarii system.

This research has made use of the WDS Catalog maintained at the U.S. Naval Observatory and Aladin and Simbad services. We thank W. I. Hartkopf for sending us recent positional data of double stars, S.M. Rucinski, E.V. Malogolovets, and Y.Y. Balega for providing us with their measurements of the visual component of V505 Sgr (by CFHT and SAO BTA telescopes), and L. Šmelcer for his photometry of V505 Sgr. We acknowledge the use of a grid of synthetic spectra prepared by J. Kubát and we thank P. Harmanec for some advice on the construction of synthetic spectra for multiple systems. This work was supported by the Czech Science Foundation (grant no. P209/10/0715) and the Research Programme MSM0021620860 of the Czech Ministry of Education. T.P. acknowledges support from the EU in the FP6 MC ToK project MTKD-CT-2006-042514.

## REFERENCES

- Applegate, J. H. 1992, *ApJ*, **385**, 621  
 Balega, I. I., et al. 2002, *A&A*, **385**, 87  
 Biermann, P., & Hall, D. S. 1973, *A&A*, **27**, 249  
 Chambliss, C. R., et al. 1993, *AJ*, **106**, 2058  
 Chochol, D., et al. 2006, *Ap&SS*, **304**, 93  
 Cook, J. M., et al. 2005, *IBVS*, **5636**, 1  
 Fernández, J. A. 2005, Comets (Dordrecht: Springer)  
 Harmanec, P. 1970, *Bull. Astron. Inst. Czech.*, **21**, 113  
 Harmanec, P., et al. 1997, *A&A*, **319**, 867  
 Hartkopf, W. I., Mason, B. D., Wycoff, G. L., & McAlister, H. 2009, <http://ad.usno.navy.mil/wds/int4.html>  
 Hill, G. 1982, *Publ. Dom. Astrophys. Obs. Victoria BC*, **16**, 67  
 Ibanoglu, C., et al. 2000, *A&A*, **354**, 188  
 Lenz, P. 2008, <http://www.astro.univie.ac.at/~dsn/dsn/Period04/>  
 Levison, H. F., & Duncan, M. J. 1994, *Icarus*, **108**, 18  
 Maksimov, A. F., et al. 2009, *Astrophys. Bull.*, **64**, 296  
 Mayer, P. 1997, *A&A*, **324**, 988  
 McAlister, H., Hartkopf, W.I., Hutter, D., & Franz, O. 1987a, *AJ*, **93**, 688  
 McAlister, H., Hutter, D., Shara, M., & Franz, O. 1987b, *AJ*, **92**, 183  
 Müyesseroglu, Z., Gürol, B., & Selam, S. O. 1996, *IBVS*, **4380**, 1  
 Paxton, B. 2004, *PASP*, **116**, 699  
 Popper, D. M. 1980, *ARA&A*, **18**, 115  
 Press, W. R., Teukolsky, S. A., Vetterling, W., & Flannery, B. P. 1997, Numerical Recipes: The Art of Scientific Computing (Cambridge: Cambridge Univ. Press)  
 Rovithis-Livaniou, H., & Rovithis, P. 1992, *IBVS*, **3803**, 1  
 Rucinski, S. M., Pribulla, T., & van Kerkwijk, M. H. 2007, *AJ*, **134**, 2353  
 Tomkin, J. 1992, *ApJ*, **387**, 631  
 Valtonen, M., & Mikkola, S. 1991, *ARA&A*, **29**, 9  
 van Leeuwen, F. 2007, *A&A*, **474**, 653  
 Worek, T. F. 1996, *PASP*, **108**, 962  
 Zasche, P., et al. 2009, *AJ*, **138**, 664